Concentration-dependent ionic conductivity and thermal stability of magnetron-sputtered nanocrystalline scandia-stabilized zirconia

M Sillassen, Per Eklund, N Pryds, N Bonanos and J Bottiger

Original Publication:

M Sillassen, Per Eklund, N Pryds, N Bonanos and J Bottiger, Concentration-dependent ionic conductivity and thermal stability of magnetron-sputtered nanocrystalline scandia-stabilized zirconia, 2010, SOLID STATE IONICS, (181), 23-24, 1140-1145.
http://dx.doi.org/10.1016/j.ssi.2010.06.010

Concentration-dependent ionic conductivity and thermal stability of magnetron-sputtered nanocrystalline scandia-stabilized zirconia

M. Sillassen[a,] *, P. Eklund[a,b], N. Pryds[c], N. Bonanos[c] and J. Bøttiger [a]

[a]*Interdisciplinary Nanoscience Center (iNANO) and Department of Physics and Astronomy, University of Aarhus, DK-8000 Aarhus C, Denmark*

[b]*Thin Film Physics Division, Department of Physics, Chemistry, and Biology, IFM, Linköping University, SE-581 83 Linköping, Sweden*

[c]*Fuel Cells and Solid State Chemistry Division, Risø National Laboratory for Sustainable Energy Technical University of Denmark - DTU, DK-4000 Roskilde, Denmark*

*Corresponding author. E-mail: mbs@phys.au.dk

Abstract

Nanocrystalline (nc) scandia-stabilized zirconia (SSZ) electrolytes with scandia contents of 5.9 to 15.9 mol% were synthesized by reactive magnetron sputtering. For scandia content ≥ 9.1 mol%, the as-deposited films were pure cubic phase with <111> texture, while traces of tetragonal phase was found for lower Sc content. Single-line profile analysis of the 111 X-ray diffraction peak yielded an out-of-plane grain size of ~10 nm and a microstrain of 2.0-2.2%, regardless of scandia content, for films deposited at 400 °C and a bias of -70 V. Films deposited at higher bias voltages showed a reduced grain size, yielding a grain size of ~6 nm and a microstrain of ~2.5% at -200 V and -250 V with additional incorporation of argon. Temperature-dependent impedance spectroscopy of the SSZ films showed that the in-plane ionic conductivity had a maximum close to 10.7 mol% and decreased almost an order of magnitude as the scandia - content was increased to 15.9 mol%. The activation energy for oxygen ion migration was determined to be between 1.30 - 1.43 eV. In addition, no

dependence on grain size was observed. The above observations suggest a bulk mechanism for ionic conduction.

Keywords: SSZ, Physical Vapor Deposition, X-ray Diffraction, Impedance Spectroscopy

1. Introduction

In solid oxide fuel cells (SOFCs), the typical thickness of the solid electrolyte layer is of the order 10-100 μm. A way of lowering the operation temperature of SOFCs could be to implement thin-film electrolytes (< 1 μm) in order to minimize the ohmic losses [1].

Progress in this area can also be achieved through identification of new solid electrolytes, which will be characterized by high ionic conductivity while the electronic contribution should be minimized. Stabilized zirconia is an exceptional material for such a study due to a high ionic conductivity and a desirable chemical stability in both oxidizing and reducing atmosphere. Electrical transport in this system comes from the oxygen vacancy concentration, which is controlled by acceptor dopants. The ionic conductivity is dependent on the size of dopants and tends to be highest for those cations whose ionic radii are closest to that of the Zr^{4+} host cation. Among the number of dopants, Sc^{3+} seems to be the most attractive due to its ionic radius of 0.87 Å, which is very close to the size of Zr^{4+} (R_{Zr}=0.84 Å). The scandia-stabilized zirconia system exhibits the highest ionic conductivity (~0.08 $\Omega^{-1}cm^{-1}$ at 800 ºC for $(ZrO_2)_{0.9}(Sc_2O_3)_{0.1}$) compared with other acceptors (as Y, Ca, Gd, Yb or Sm) in the intermediate temperature range 650-850 ºC [2, 3]. For this reason, SSZ has been considered as an alternative for YSZ, which has typically been the material of choice for electrolytes in SOFCs.

The scandia-zirconia system is rather complex, since seven phases are known in the zirconia - rich part of the phase diagram. In addition to the pure zirconia phases (monoclinic, tetragonal and cubic), there is a metastable tetragonal-rich *t'* phase, and ordered β ($Sc_2Zr_7O_{17}$), γ ($Sc_2Zr_5O_{13}$), and δ ($Sc_4Zr_3O_{12}$) rhombohedral phases [4]. The existence of these phases comes from the small difference in the ion radius between the Sc^{3+} dopant and the Zr^{4+} host cation, and hence a small barrier for redistribution of the dopants. This means that the crystal structure, and hence properties, of the SSZ films are highly sensitive to the synthesis method and the thermal history [5]. An

enhancement in ionic conductivity was found in sol-gel derived nanocrystalline 8SSZ (8.0 mol% Sc_2O_3) thin films, due to grain size effects [6, 7]. In our previous work on magnetron-sputtered nc-YSZ, we observed a similar correlation between ionic conductivity and grain size [8]. Furthermore, we observed several orders conductivity enhancement in epitaxial YSZ grown on MgO and $SrTiO_3$ single crystals in a recent work [9]. Studies of the mechanisms for ionic conduction in nanomaterials [10, 11] have shown that the mobility of ions can be increased through grain boundaries and interfaces, resulting in orders of magnitude greater diffusivity [12, 13].

In this paper, we investigate the structure and the correlation to the in-plane ionic conductivity of nanocrystalline SSZ thin films synthesized by reactive pulsed DC magnetron sputtering. The activation energy for oxygen ion migration was similar to reported values for bulk migration in SSZ.

2. Experimental details

SSZ films were deposited by reactive pulsed DC magnetron sputtering from a pure 2-inch Zr target with strips of Sc attached. Si(001) substrates (15x15 mm^2) with native oxide layers were used. In addition, non-conducting quartz SiO_2(001) substrates (20x6 mm^2) were used for the films intended for in-plane ionic conductivity measurements. All substrates were ultrasonically cleaned in acetone and ethanol and blown dry with nitrogen. The details on the growth chamber are described in [8]. A deposition rate of ~ 4.5 nm/min was obtained at a working pressure of 0.5 Pa with a gas-mixture of Ar (99.9996%) and O_2 (99.9999%) with an Ar:O_2 flow-ratio of 9.0:0.7 sccm (standard cubic centimeters per minute). The power density to the target was ~1.4 W/cm^2. In order to have a stable process with a reasonably high deposition rate, films were synthesized in the metallic mode. The deposition time was 30 min corresponding to a film thickness ~130 nm.

The sampling depth and chemical composition were determined by Rutherford backscattering spectroscopy (RBS) using 2 MeV $^4He^+$ ions and a scattering angle of 161º. The experimental data were simulated with the RUMP program [14], from which film thicknesses were obtained using an empirical film density. From a cautious estimate based on thicknesses obtained from RBS and XSEM (cross section), the films are roughly 10% less dense than their bulk counterparts. Within the measurement accuracy, RBS showed that the film thickness had little dependence on temperature and bias variation. X-ray diffraction (XRD) measurements in θ-2θ and grazing incidence (GIXRD) geometry (5º incidence) were performed with a Bruker D8 Discover diffractometer using CuKα radiation. Single-line profile analysis was performed with the software package TOPAS 2.1 [15] using a pseudo-Voigt peak profile [16]. The size of the coherently diffracting domains, which has been used as a measure for the average grain size, and the microstrain were determined from the integral breadths of the Lorentzian and Gaussian constituents of the pseudo-Voigt function, respectively. Scanning electron microscopy (SEM) was performed in an FEI NOVA 600 SEM with accelerating voltage 5 kV and working distance 4 mm. Transmission electron microscopy (TEM) was performed in a Philips CM20 TEM working at 200 kV.

Annealing was carried out in a quartz tube oven with a flow of pure nitrogen (1 l/min). The samples were placed on a quartz boat, which was placed at the centre of the preheated oven and annealed for 1 h. The temperature was measured with a thermocouple placed near the samples inside the oven (error ± 10 °C). After annealing, the samples were cooled down for 1 h before they were taken out of the oven, so the samples would not be exposed to thermal shock. This procedure was repeated for annealing temperatures of 600, 750, 1000, and 1200 ºC.

Impedance spectroscopy measurements were carried out with films on quartz substrates in a dry-air atmosphere oven, using a four-terminal pair configuration with Ag electrodes painted on top to which leads were attached. The separation between the Ag electrodes was 1.5 mm.

Measurements were performed at temperatures from 750 ºC down to 450 ºC in steps of 50 ºC (10 ºC/min) and a dwell time of 30 min to ensure steady state conditions at each measuring point. A Hioki 3250-50 frequency analyzer in the range 42 Hz – 1 MHz was used and the impedance data were analyzed with the software ZSimpWin 3.21 [17]. Note that even though we have done AC measurements, the lateral geometry allowed us only to resolve the total conductivity, and not the grain interior and grain boundaries.

3. Results and discussion

Fig. 1 shows θ-2θ X-ray diffractograms for films deposited at 400 °C and -70 V bias with different scandia concentrations. The film with a scandia content of 5.9 mol% exhibits peaks corresponding to tetragonal and cubic zirconia phases. At a scandia content of 9.1 mol% and higher, only peaks corresponding to the pure cubic zirconia phase are observed. In Fig. 1, the 111 peak is dominant for the samples in the cubic phase, showing that these films have a <111> texture. The <111> film texture is likely to develop due to the low surface energies of <111> oriented grains [18]. Fig. 2 shows the out-of-plane grain sizes and microstrains in cubic SSZ samples, deposited at 400 °C and -70 V, determined from the 111 diffraction peak (θ-2θ) as a function of the scandia concentration. The out-of-plane grain sizes and microstrains exhibit only a weak dependence on the scandia concentration. This could be due to the similarity of the ion radii of the Sc^{3+} dopant and the Zr^{4+} host cation. The observed tendency is confirmed from the TEM images (Fig. 3) of two samples, deposited at 400 °C and -70 V, with scandia concentrations of (a) 5.9 mol% and (b) 10.7 mol%, respectively. From Fig. 3(a), the estimated average (in-plane) grain size for the sample containing 5.9 mol% Sc_2O_3, corresponding to a mixed tetragonal and cubic phase (cf. Fig. 1), is $\overline{D}$ ~ 11 nm. From Fig. 3(b), an estimated average grain size of $\overline{D}$ ~ 13 nm is obtained for the sample containing 10.7 mol% Sc_2O_3, which is completely stabilized in the cubic phase (cf. Fig. 1).

Cubic SSZ films with scandia concentrations varying from 9.1 mol% to 12.3 mol% were deposited with an applied substrate bias in the range -70 V to -250 V. From the θ-2θ scans (similar to those shown in Fig. 1), all samples showed a <111> texture regardless of substrate bias. Fig. 4 shows the out-of-plane grain sizes and microstrains obtained from single-line profile analysis of the 111 peak as a function of bias voltage (for scandia concentrations within the range 9.1 - 12.3 mol%). At floating potential, the grain size is ~11.5 nm and decreases to ~ 6 nm for films deposited at -200 V and -250 V. This is due to the ion-bombardment-induced formation of more nucleation

centers. The microstrain remains constant at ~1.5% for samples deposited at floating potential, -70 V and -100 V. For samples deposited at -150 V, -200 V, and -250 V, the bombarding Ar^+ ions induced radiation damage as indicated by the increase in microstrain. Generally, Ar impurities from the process gas were incorporated in the films when a substrate bias of -70 V or higher was applied during deposition. The samples deposited at -70 V, -100 V, -150 V, -200 V, and -250 V had Ar contents of 1.0, 1.2, 1.7, 2.3, and 2.8 at.%, respectively, as determined by RBS. Furthermore, all films were found to be stoichiometric in oxygen according to the formula $(ZrO_2)_{1-2x}(Sc_2O_3)_x$. The structural and compositional analysis for SSZ films deposited on quartz revealed no significant differences from those deposited on Si.

The Arrhenius expression relating ionic conductivity, σ, and absolute temperature, T, is given by

$$\sigma T = A \exp(-E_a/k_B T), \quad (1)$$

where A is the pre-exponential coefficient, E_a is the activation energy for oxygen ion migration, and k_B is the Boltzmann constant, respectively.

Fig. 5 shows plots of $\ln(\sigma T)$ vs. $10000/T$ for samples, deposited at 400 °C and -70 V bias, with scandia concentrations of 9.1, 10.7, 11.9, 14.3, and 15.9 mol%. All data sets follow an Arrhenius-like behaviour. Least-squares-fitting yielded slopes, from which activation energies for oxygen ion migration in the range 1.30 - 1.43 eV were obtained (Eq. 1). Within the standard deviations the activation energies were found to be the same, regardless of scandia-concentration. These values are similar to the activation energy for migration in bulk SSZ [19, 20]. Badwal *et al* obtained activation energies in the range ~1.25 - 1.39 eV for bulk samples with scandia concentrations ranging from 7 to 11 mol% [20]. It is observed from Fig. 5 that the film conductivity is highest for the sample with 10.7 mol% Sc_2O_3. The lower conductivity of the sample with 9.1

mol% Sc_2O_3 is most likely due to a lower concentration of oxygen vacancies. For samples with higher scandia concentrations, the drop in ionic conductivity may be related to possible phase transitions to one of the ordered rhombohedral phases in the scandia-zirconia system. This is elaborated below.

The inset in Fig. 5 shows representative impedance spectra at 636, 689, and 737 ºC for the sample with a scandia concentration of 10.7 mol%. The spectra consist of only one semicircle, attributed to the sample response, which is slightly asymmetric in the low frequency range. An equivalent $(RQ)R$ circuit was used in the fitting procedure to obtain the resistances R, with Q representing a constant phase element. The observed response is most likely a superposition of parallel mechanisms for ionic conduction, i.e. bulk migration and grain boundary migration.

Fig. 6(a, b) show ln(σ) vs. scandia concentration at a measuring temperature of 590 °C and 490 °C, respectively, for the SSZ films and corresponding bulk materials [21]. The absolute conductivities in this study lie below the bulk conductivities obtained by Huang *et al* [21]. The reason for this is most likely due to the different structures (micro- or nanostructure) in addition to possible impurities at the grain boundaries. As mentioned, the film conductivity is highest for the sample with 10.7 mol% Sc_2O_3 and drops one order of magnitude for samples with 14.3 and 15.9 mol% Sc_2O_3. It is observed that the ionic conductivities for the bulk samples [21] drop off much faster than for the films with higher Sc content at a measuring temperature of 590 °C (Fig. 6a). At a measuring temperature of 490 °C (Fig. 6b) the in-plane ionic conductivity for the SSZ films in the present study show the same relative tendency as a function of scandia concentration. However, the ionic conductivities for the bulk samples, obtained by Huang *et al* [21], show a maximum at a lower scandia concentration. This discrepancy may again be due to different structures and possible grain-boundary impurities.

This type of drop in ionic conductivity has been linked to a phase transition that occurs between the cubic and the ordered rhombohedral phases (β, γ, and δ) near 600 °C for SSZ with a doping level of ≥ 10 mol% [22]. Fig. 7 shows θ-2θ X-ray diffractograms of the sample with highest scandia content (15.9 mol%), deposited at 400 °C and -70V, as deposited and at annealing temperatures of 600, 750, 1000, and 1200 ºC. The as-deposited sample is stabilized in the cubic phase with a preferred <111> orientation. However, at annealing temperatures of 600 and 750 °C, the 111 diffraction peak becomes more asymmetric suggesting the beginning of a phase transition, and at annealing temperatures of 1000 and 1200 °C the transition to the ordered rhombohedral γ-phase ($Sc_2Zr_5O_{13}$) is complete. During the present impedance measurements, all samples were initially heated to ~750 °C and cooled down in steps of 50 °C between successive measurements, which means that the SSZ films with a scandia content of 14.3 and 15.9 mol% likely have undergone a phase transition to one of the ordered rhombohedral phases in the scandia - zirconia system.

Fig. 8 shows (a) surface view and (b) cross-section SEM images of the annealed sample, i.e. the sample with 15.9 mol% Sc_2O_3, after the final annealing step at 1200 ºC. Annealing results in grain coarsening ($\overline{D}$ ~ 50 nm) as seen from Fig. 8(a), however, no visible cracking of the film can be seen from either view (Fig. 8(a,b)). Furthermore, the sample shows good adherence to the Si substrate after annealing (Fig. 8(b)). Hence, the conductivities reported here should not be influenced by mechanical cracks in the films or film delamination. Based on earlier studies of the thermal stability of magnetron-sputtered YSZ films [8], we also consider grain growth in the films as negligible below an annealing temperature of 800 ºC, and grain growth should therefore not be an issue for the ionic-conductivity measurements performed here.

Fig. 9 shows ln(σT) vs. 10000/T for two samples with roughly the same composition, both deposited at 400 °C, but with a bias of -70 V and -100 V, respectively. A minor difference in the in-

plane ionic conductivities is observed between the samples, suggesting that grain size effects are limited and that the ionic conduction in the SSZ films is dominated by bulk migration despite grain sizes of the order ~10 nm. This is different to what we have previously observed for magnetron-sputtered nanocrystalline yttria-stabilized zirconia (YSZ) thin films [8], whose in-plane ionic conductivity depended on the grain size. In this paper [8] we motivated the idea that oxygen ions may migrate through a superposition of bulk and grain-boundary effects. In the present study, it was observed that the in-plane ionic conductivities of the nc-SSZ films were higher than for corresponding nc-YSZ thin films with the same doping level [8].

The ionic-conductivity results for the present magnetron-sputtered nanocrystalline SSZ films differ from the observations by Kosacki *et al* [5] and Zhang *et al* [6] where a considerable enhancement of ionic conduction was seen in sol-gel derived nanocrystalline SSZ thin films as the grain size was reduced. Zhang *et al* attributed this enhancement to a decrease in grain boundary resistance due to interfacial effects between grains and grain boundaries, and even though they found an activation energy for grain-boundary oxygen ion migration higher than that of the bulk, they argued that, as the grain size is reduced to the nanometer regime, interfacial effects between the grains and grain boundaries may become prominent. Under this condition, dopants distributed between grains and grain boundaries during processing may sharply increase the nonstoichiometry level of the films. As a result, the speed of the oxygen ions across or along the grain boundaries is accelerated, giving rise to an enhanced conductivity. The reasoning is further supported by our recent work on single epitaxial YSZ layers grown on $SrTiO_3$ and MgO single crystals [9]. In this paper, high lateral ionic conductivity enhancements were demonstrated at low temperatures. The source of this enhancement was found at the interfaces due to the combined effect of strain and misfit dislocations [9]. Furthermore, Garcia-Barriocanal *et al* produced heterostructures of ultrathin multilayers of YSZ and $SrTiO_3$ and observed up to eight orders magnitude enhancement of the ionic

conductivity of YSZ compared to bulk values [23]. The high ionic conductivity was enabled by the absence or displacement of oxygen positions in the interface planes of the perovskite ($SrTiO_3$) and fluorite (YSZ) structures. These heterostructures serve, in a way, as a model system for a nanocrystalline material and thus illustrates the possible implications of nonstoichiometry in nanocrystalline materials. Recently, the results obtained by Garcia-Barriocanal *et al* [23, 25] have been questioned by Guo [24], who argues that the observed enhancement in ionic conductivity [23] is probably due to the *p*-type conductivity of $SrTiO_3$. Guo's argument is, however, contradicted by our results [9] where an enhancement in ionic conductivity of several orders of magnitude was found also on (non-conducting) MgO single crystals.

In the present study, the structure at the grain boundaries may be different due to additional ion bombardment of the growing film. The level of nonstoichiometry at the grain boundaries may be important for magnetron-sputtered nc-YSZ [8], but does not seem to play a dominant role for magnetron-sputtered nc-SSZ. This observation may be due to the similarity of the ion radii of the Sc^{3+} dopant and the Zr^{4+} host cation. However, in each case the activation energies for oxygen ion migration are found to lie above the values for single crystal YSZ and SSZ, respectively. These results suggest that in our SSZ films, in-plane ionic conduction predominantly occurs through bulk migration, despite their nanocrystalline structure with grain sizes of ~10 nm. A further argument for bulk migration in magnetron-sputtered nc-SSZ films is the dependence on the in-plane ionic conductivity of the scandia concentration (cf. Fig. 6(a,b)). The in-plane ionic conductivity had a maximum close to 10 mol% scandia similar to what has been observed for bulk SSZ.

The reason for the bulk-like ionic conduction in the present nanocrystalline SSZ films may be the incorporation of Ar during film growth from the additional ion bombardment at the substrate. The Ar impurities may segregate to the grain boundaries, thereby blocking these particular pathways for the O^{2-} ions.

4. Conclusion

This work has shown that the in-plane ionic conductivity of magnetron-sputtered nanocrystalline SSZ films is highly dependent on the amount of scandia in the films. Generally, the scandia - rich samples had lower conductivities probably due to a phase transition at higher temperatures to one of the ordered rhombohedral phases during the impedance measurements. Activation energies for oxygen migration in the range 1.30 - 1.43 eV, similar to bulk migration, were obtained. Additionally, no grain size effects on the in-plane ionic conductivity were observed. These results suggest that ionic conduction predominantly occurs through bulk migration, despite the nanocrystalline structure, maybe due to grain-boundary impurities.

Acknowledgments

The authors would like to thank the Danish Ministry of Science for financial support. P. E. acknowledges funding from the Carlsberg Foundation, the Swedish Research Council (VR), and the Swedish Foundation for Strategic Research (SSF).

References

[1] S. A. Barnett, Energy **15** (1990) 1.
[2] S.P.S. Badwal, Solid State Ionics **52** (1992) 23.
[3] S. M. Haile, Acta Mater. **51** (2003) 5981.
[4] M.R. Thirnber, D.J.M. Bevan, J. Graham, Acta Crystallogr. B **24** (1968) 1883.
[5] C. Haering, A. Roosen, H. Schichl, M. Schnoller, Solid State Ionics **176** (2005) 261.
[6] I. Kosacki, H.U. Anderson, Y. Mizutani, K. Ukai, Solid State Ionics **152–153** (2002) 431.
[7] Y.-W. Zhang, S. Jin, Y. Yang, G.B. Li, S.J. Tian, J.T. Jia, C.-S. Liao, C.-H. Yan, Appl. Phys. Lett. **77** (2000) 3409.
[8] M. Sillassen, P. Eklund, M. Sridharan, N. Pryds, N. Bonanos, and J. Bøttiger, J. Appl. Phys. **105**, 104907 (2009).
[9] M. Sillassen, P. Eklund, N. Pryds, E. Johnson, U. Helmersson, and J. Bøttiger, Accepted for publication in Adv. Func. Mater.
[10] J. Maier, Solid State Ionics **131** (2000) 13.
[11] H. Tuller, Solid State Ionics **131** (2000) 143.
[12] G. Knöner, K. Reimann, R. Röwer, U. Södervall, and H.-E. Schaefer, Proc. Natl. Acad. Sci. U.S.A. **100**, No. 7 (2003) 3870.
[13] U. Brossman, G. Knöner, H.-E. Schaefer, and R. Würschum, Rev. Adv. Mater. Sci. **6** 7 (2004) 7.
[14] L. R. Doolittle, Nucl. Instrum. Methods Phys. Res., B Beam Interact. Mater. Atoms **9** (1985) 344.
[15] Diffrac^{plus} Topas P 2.1, Bruker AXS GmbH D-76187 Karlsruhe, Germany (2003).
[16] Th. H. de Keijser, J. I. Langford, E. J. Mittemeijer, and A. B. P. Vogels, J. Appl. Crystallogr. **15** (1982) 308.
[17] ZSimpWin 3.21, EChem Software, Bruno Deum, Ann Arbor, Michigan, USA, 1999-2005.
[18] I. Petrov, P. B. Barna, L. Hultman, and J. E. Greene, J. Vac. Sci. and Technol. A **21**, 5 (2003) 117.
[19] F. Hund, Z. Phys. Chem. **199** (1952) 142.
[20] S. P. S. Badwal, F. T. Ciacchi, D. Milosevic, Solid State Ionics **136-137**, (2000) 91.
[21] H. Huang, C.-H. Hsieh, N. Kim, J. Stebbins, F. Printz, Solid State Ionics **179**, (2008) 1442.
[22] Y. Arachi, H. Sakai, O. Yamamoto, Y. Takeda, N. Imanishai, Solid State Ionics **121**, (1999) 133.
[23] J. Garcia-Barriocanal, A. Rivera-Calzada, M. Varela, Z. Sefrioui, E. Iborra, C. Leon, S. J. Pennycook, and J. Santamaria, Science **321**, (2008), 676.
[24] X. Guo, Science **324**, (2009), 465a.
[25] J. Garcia-Barriocanal, A. Rivera-Calzada, M. Varela, Z. Sefrioui, E. Iborra, C. Leon, S. J. Pennycook, and J. Santamaria, Science **324**, (2009), 465b.

Figure Captions

FIG. 1 θ-2θ X-ray diffractograms of SSZ samples, deposited at 400 °C and -70V, with different scandia concentrations. C*** represents index of cubic crystal, but only the clearest peaks are indicated. *t* refers to tetragonal phase.

FIG. 2 Out-of-plane grain size and microstrain vs. scandia concentration for the 111 diffraction peak in the θ-2θ geometry. The error bars represent the estimated standard deviations when fitting the X-ray data to a pseudo-Voigt function.

FIG. 3 Dark field (plan-view) TEM images of the samples, deposited at 400 °C and -70V, with scandia concentrations of (a) 5.9 mol% and (b) 10.7 mol%.

FIG. 4 Out-of-plane grain size and microstrain vs. substrate bias for the 111 diffraction peak in the θ-2θ geometry for scandia concentrations (substrate bias) of: 11.7 (floating), 11.9 (-70 V), 11.4 (-100 V), 12.3 (-150 V), 10.9 (-200 V), and 9.1 mol% (-250 V). The error bars represent the estimated standard deviations when fitting the X-ray data to a pseudo-Voigt function.

FIG. 5 Arrhenius plots showing the in-plane ionic conductivity vs. inverse temperature for films, deposited at 400 °C and -70 V, with different scandia concentrations. The activation energies for oxygen migration are indicated in the legend for each sample. The error bars have been calculated from the measuring geometry and the standard deviation of the resistance. The unit for σ is S/cm. The inset shows representative impedance spectra measured at 636, 689, and 737 ºC for the sample with a scandia concentration of 10.7 mol%.

FIG. 6 (a) ln(σ) vs. scandia concentration at a measuring temperature of 590 °C and (b) 490 °C. The solid lines are guides to the eye. The error bars have been calculated from the measuring geometry and the standard deviation of the resistance. The unit for σ is S/cm.

FIG. 7 θ-2θ X-ray diffractograms of the sample with highest scandia content (15.9 mol%), deposited at 400 °C and -70V, at different annealing temperatures. C represents a cubic crystal, and * represents the rhombohedral γ-phase. Only the clearest peaks are indicated.

FIG. 8 (a) Surface view and (b) cross-section SEM images of the sample with a scandia content of 15.9 mol% Sc_2O_3 (cf. Fig. 7) after final annealing at 1200 ºC. The scale bar applies to both SEM images.

FIG. 9 ln(σT) vs. 1000/T for two samples with compositions of 11.9 and 11.4 mol% Sc_2O_3, both deposited at 400 °C, but with a bias of -70 V and -100 V, respectively. The unit for σ is S/cm.

Figure1

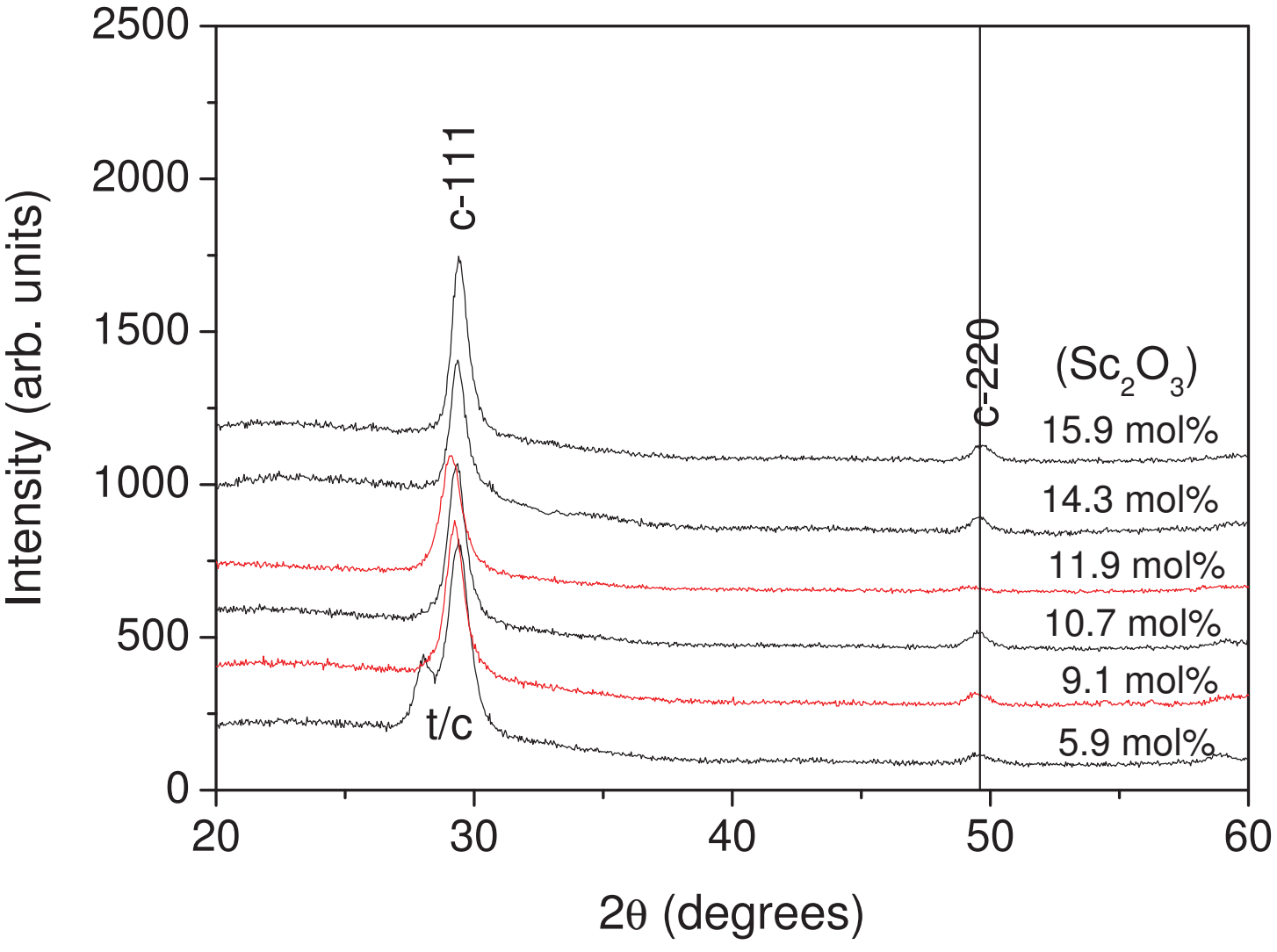
2500
2000
1500
1000
500
0
Intensity (arb. units)
c-111
c-220
t/c
(Sc2O3)
15.9 mol%
14.3 mol%
11.9 mol%
10.7 mol%
9.1 mol%
5.9 mol%
20
30
40
50
60
2θ (degrees)

Figure2

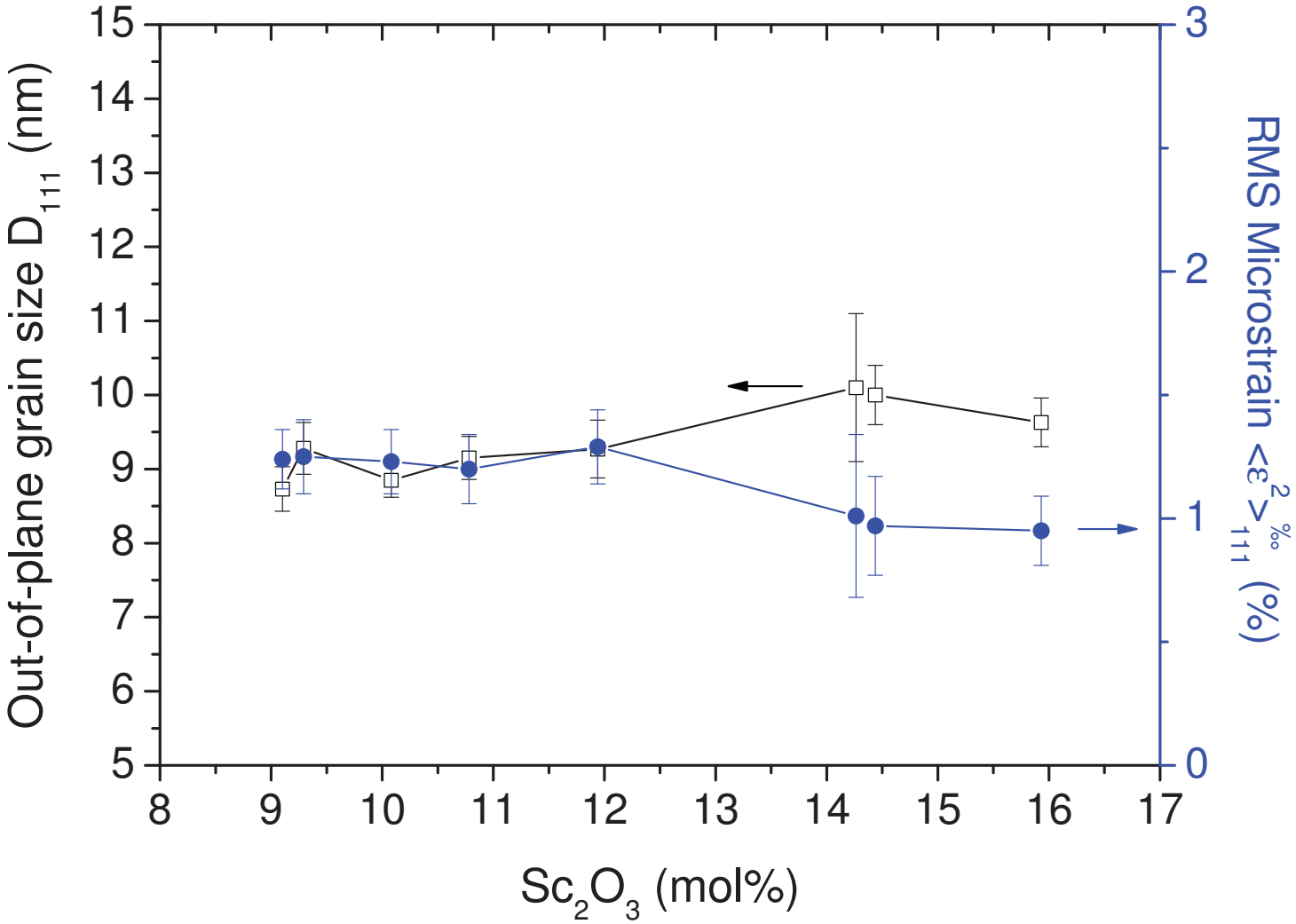
Out-of-plane grain size D_{111} (nm)
RMS Microstrain $\langle \varepsilon^2 \rangle^{\%}_{111}$ (%)
Sc_2O_3 (mol%)
15
14
13
12
11
10
9
8
7
6
5
3
2
1
0
8
9
10
11
12
13
14
15
16
17

Figure3
Click here to download high resolution image

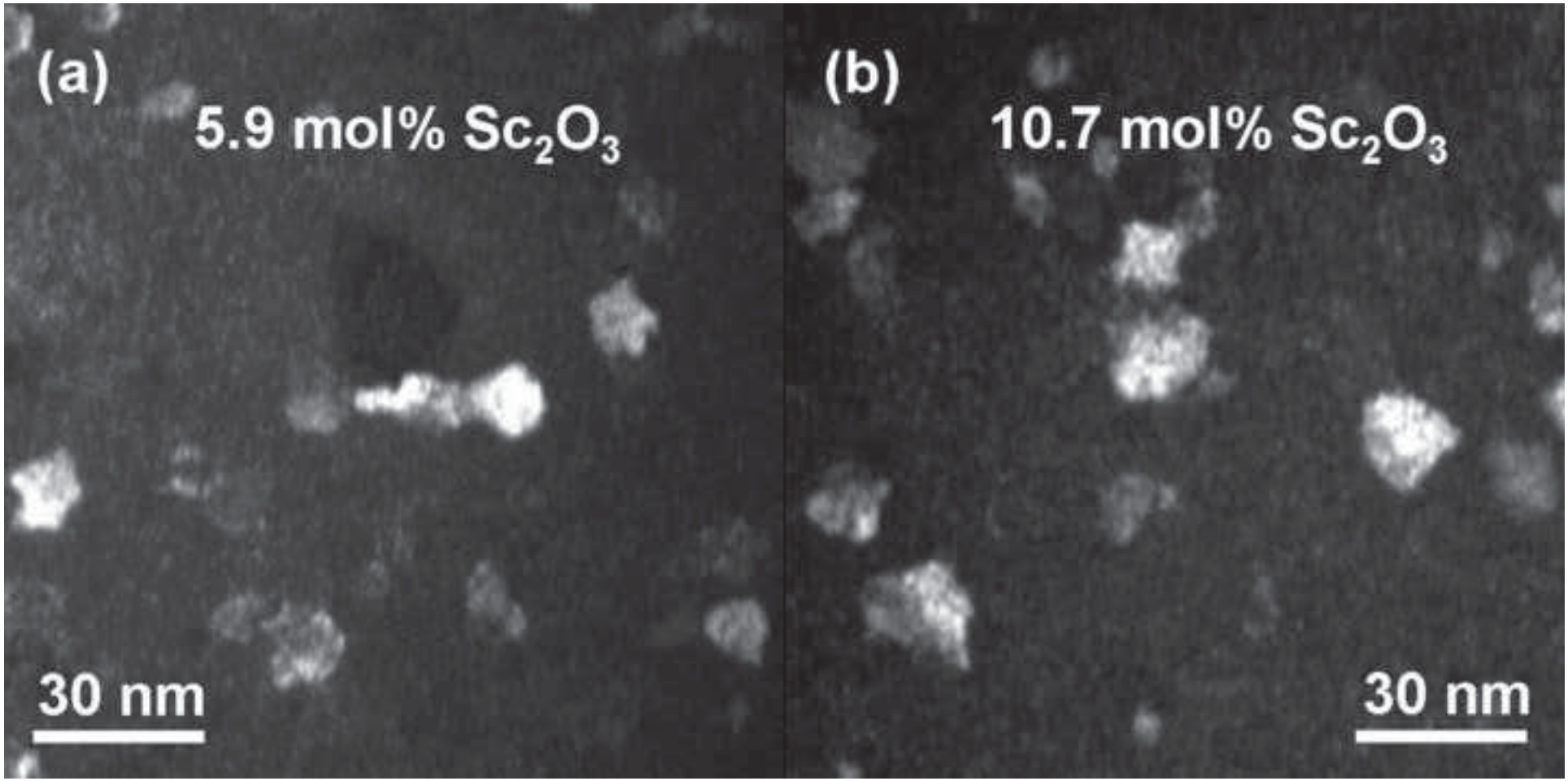

Figure4

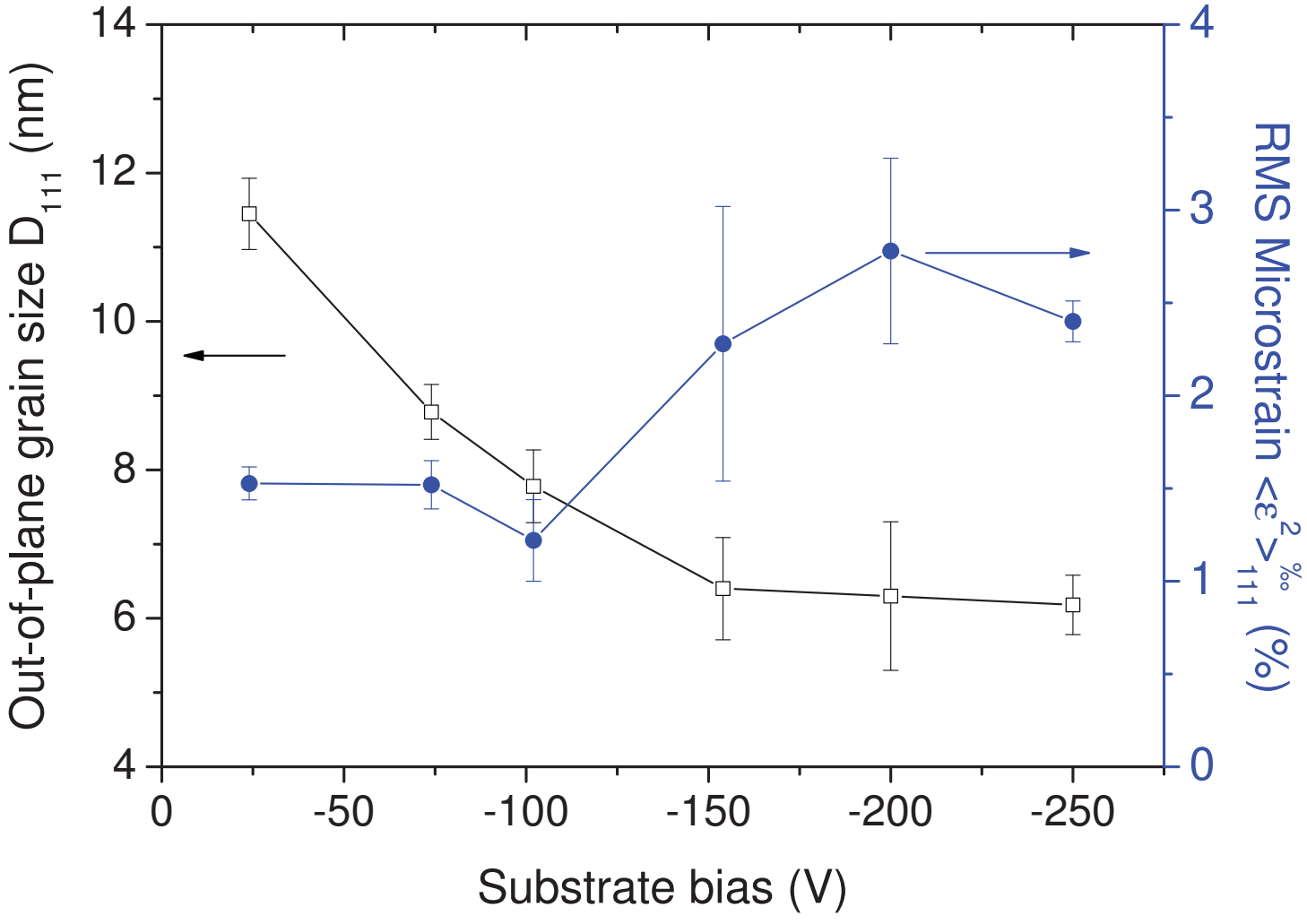
Out-of-plane grain size D_{111} (nm)
RMS Microstrain $\langle \varepsilon^2 \rangle_{111}^{\%\%}$ (%)
Substrate bias (V)
14
12
10
8
6
4
4
3
2
1
0
0
-50
-100
-150
-200
-250

Figure5

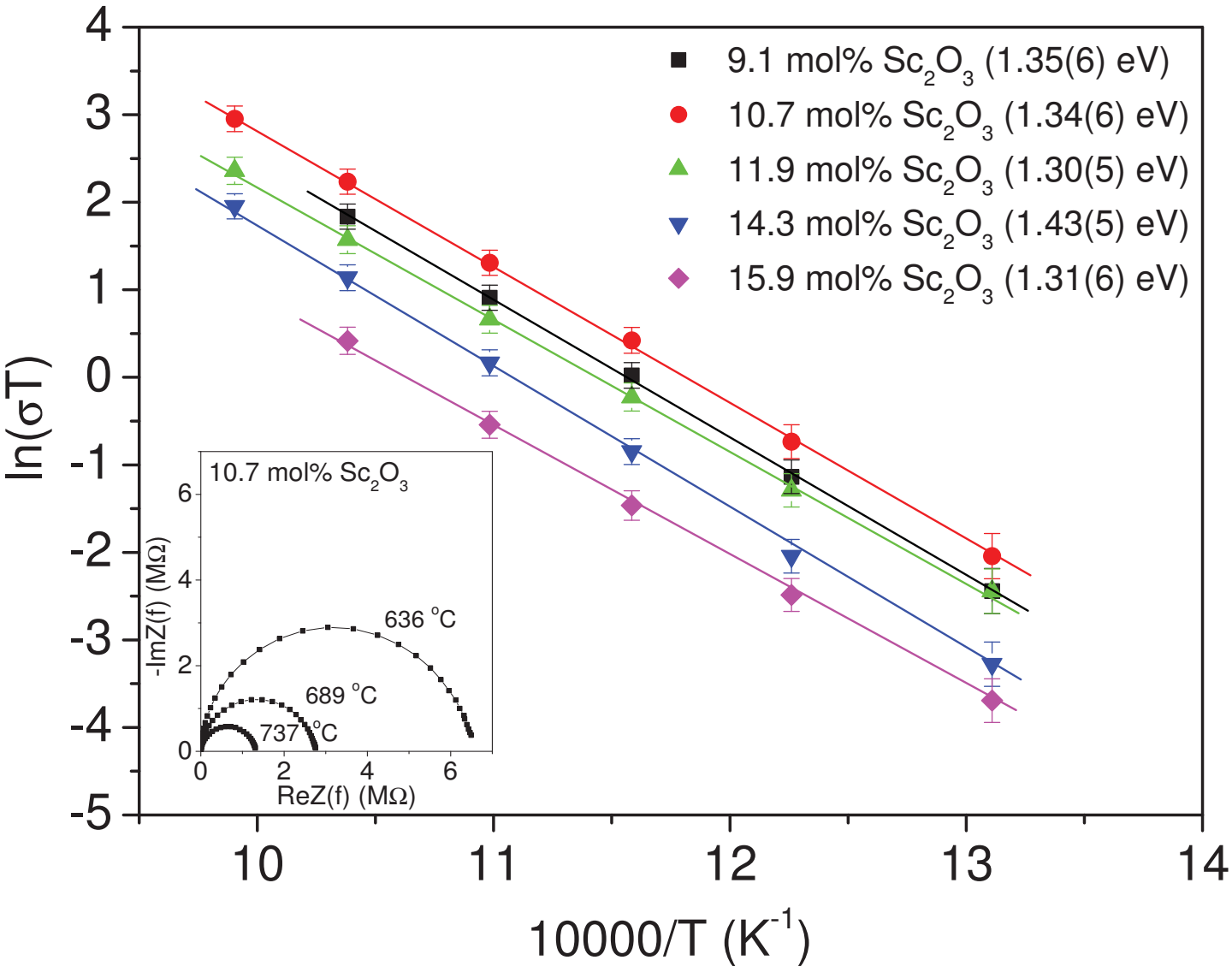
9.1 mol% Sc2O3 (1.35(6) eV)
10.7 mol% Sc2O3 (1.34(6) eV)
11.9 mol% Sc2O3 (1.30(5) eV)
14.3 mol% Sc2O3 (1.43(5) eV)
15.9 mol% Sc2O3 (1.31(6) eV)
ln(σT)
10000/T (K-1)
10.7 mol% Sc2O3
-ImZ(f) (MΩ)
ReZ(f) (MΩ)
636 °C
689 °C
737 °C

Figure6

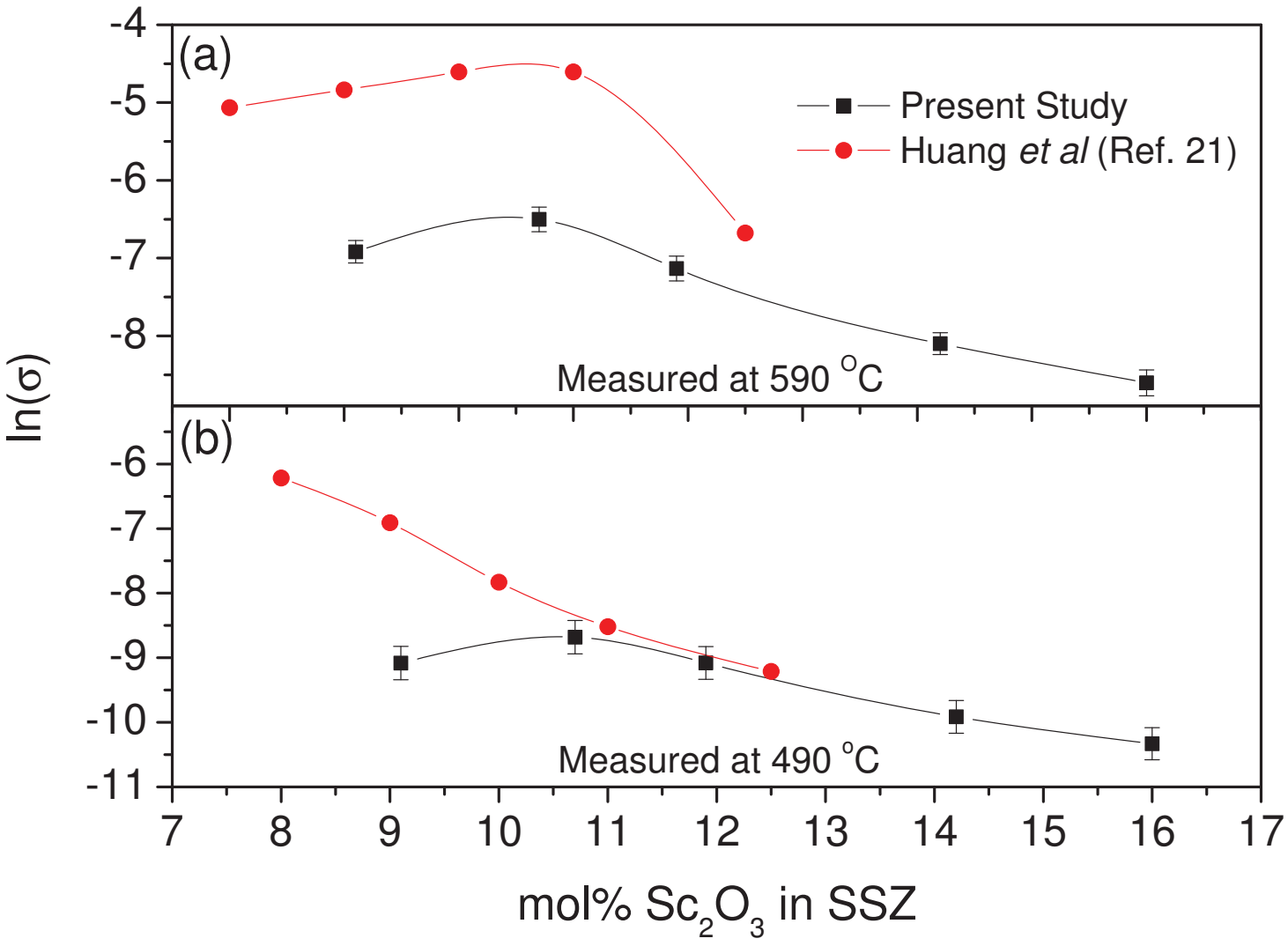
(a)
(b)
Present Study
Huang et al (Ref. 21)
Measured at 590 °C
Measured at 490 °C
ln(σ)
mol% Sc2O3 in SSZ
-4
-5
-6
-7
-8
-9
-10
-11
7
8
9
10
11
12
13
14
15
16
17

Figure7

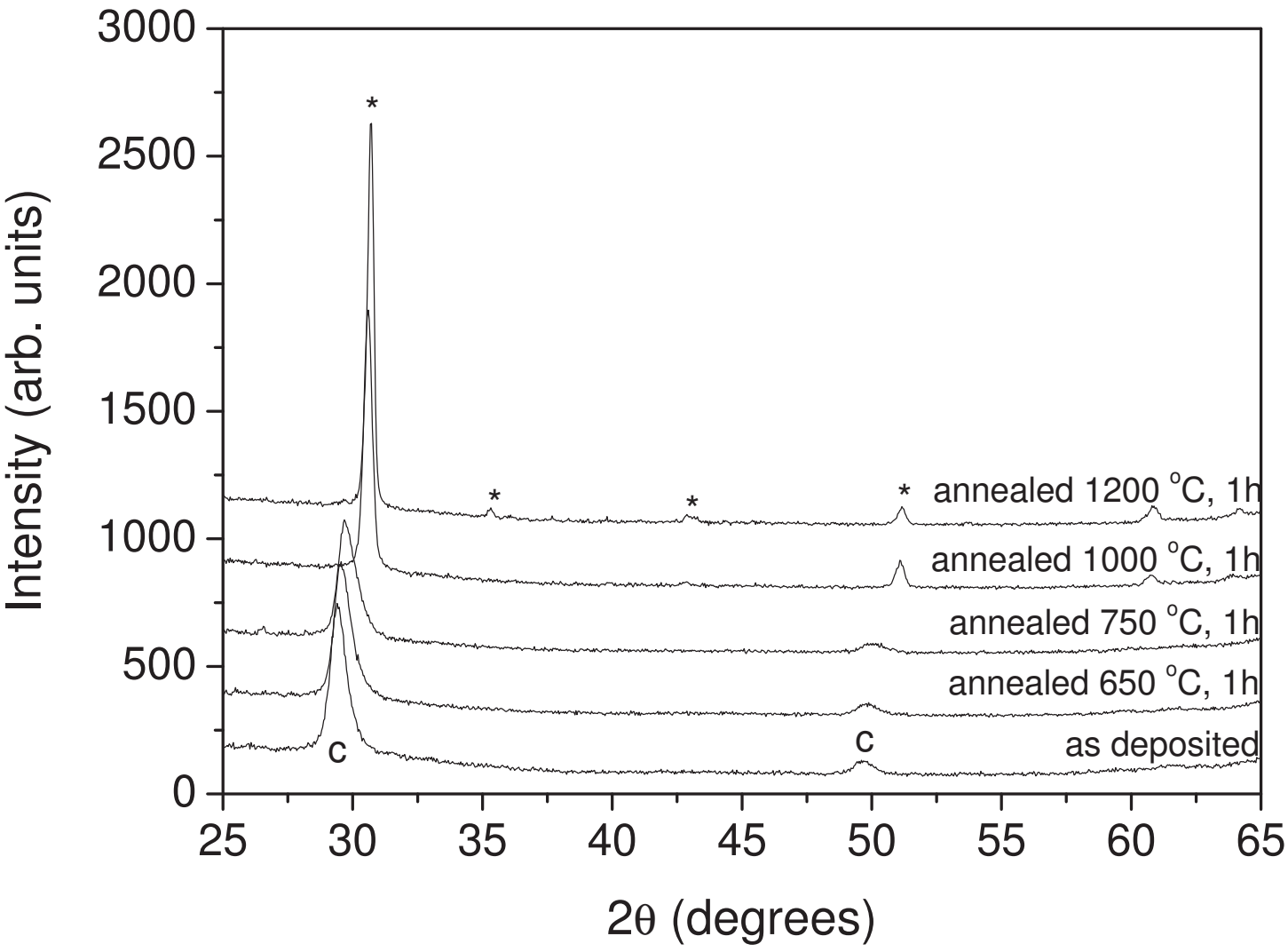
Intensity (arb. units)
3000
2500
2000
1500
1000
500
0
25
30
35
40
45
50
55
60
65
2θ (degrees)
annealed 1200 °C, 1h
annealed 1000 °C, 1h
annealed 750 °C, 1h
annealed 650 °C, 1h
as deposited
*
*
*
*
c
c

Figure8
Click here to download high resolution image

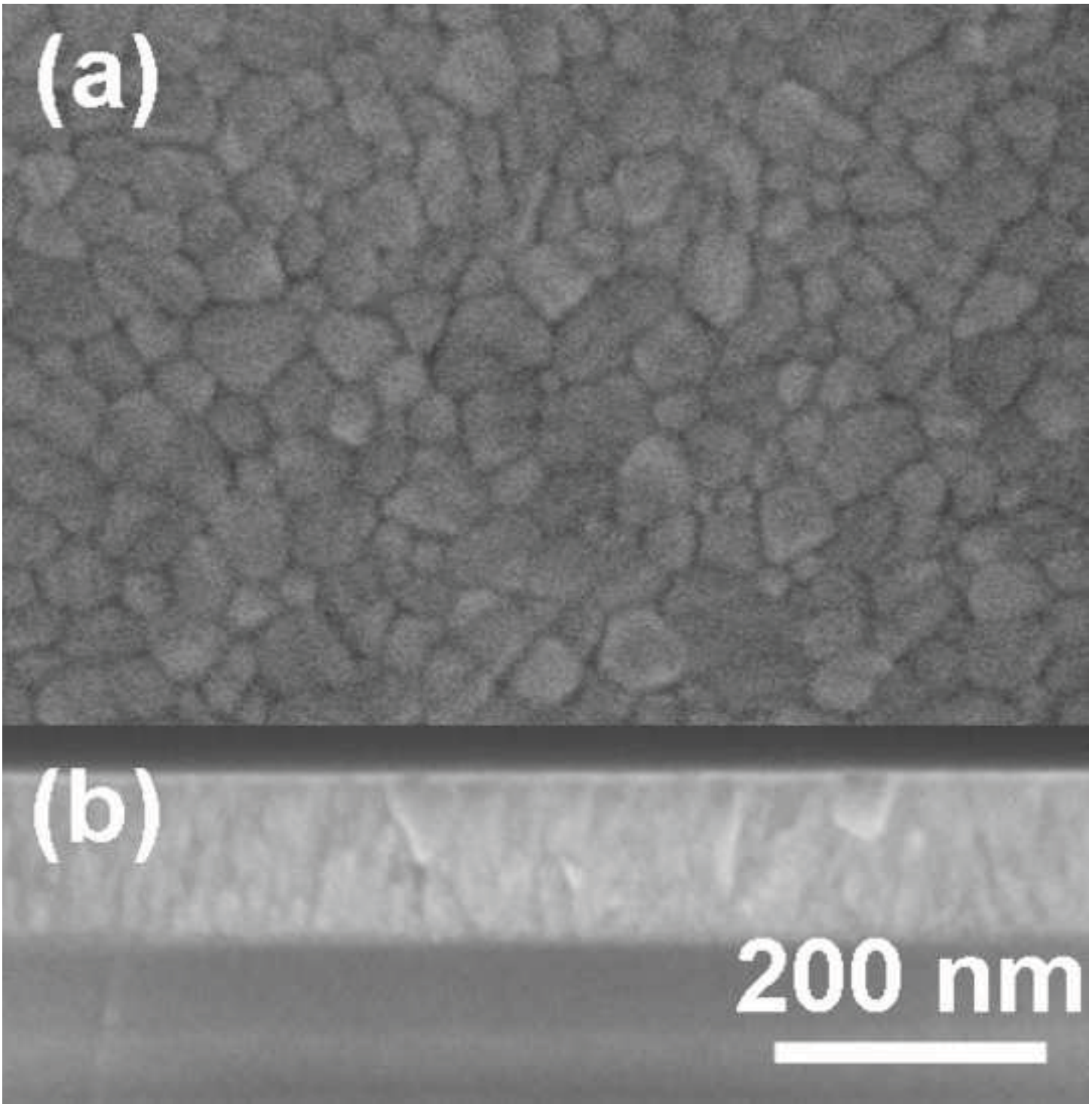

Figure9

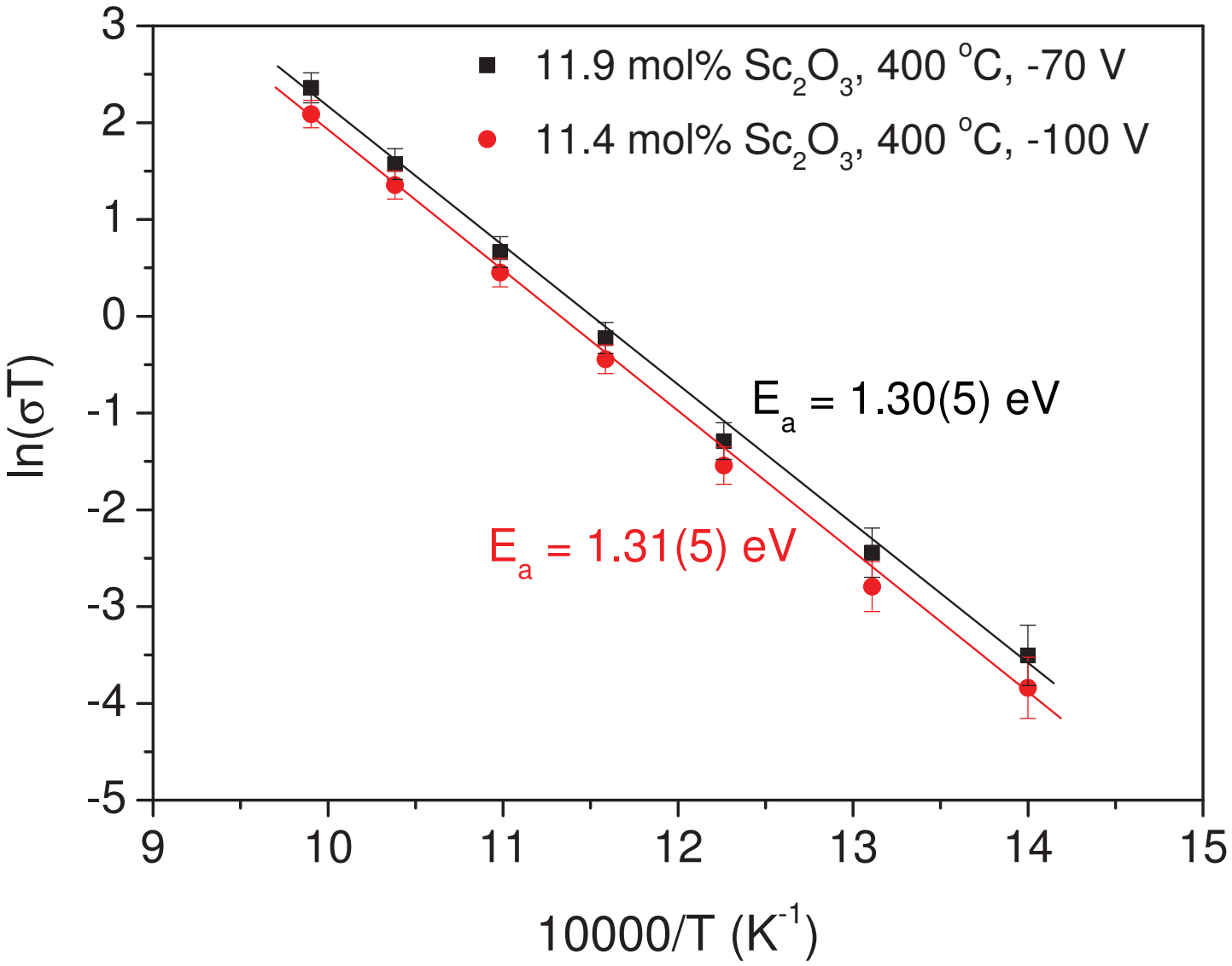
11.9 mol% Sc2O3, 400 °C, -70 V
11.4 mol% Sc2O3, 400 °C, -100 V
Ea = 1.30(5) eV
Ea = 1.31(5) eV
ln(σT)
10000/T (K-1)
3
2
1
0
-1
-2
-3
-4
-5
9
10
11
12
13
14
15